



1 **Impacts of Three Gorges Dam’s operation on spatial-temporal**
2 **patterns of tide-river dynamics in the Yangtze River estuary, China**

3 Huayang Cai^{1, 2}, Xianyi Zhang¹, Leicheng Guo², Min Zhang^{3,*}, Feng Liu¹, Qingshu
4 Yang¹

5
6 1. *Institute of Estuarine and Coastal Research, School of Marine Engineering and*
7 *Technology, Sun Yat-sen University, Guangzhou, China*

8 2. *State Key Laboratory of Estuarine and Coastal Research, East China Normal*
9 *University, Shanghai, China*

10 3. *Shanghai Normal University, School of Environmental and Geographical Sciences,*
11 *Shanghai, China*

12 **Corresponding author:** Min Zhang

13 **Corresponding author’s E-mail:** zhangmin@shnu.edu.cn

14

15 **Key points**

16 1. Impacts of TGD’s operation on tide-river dynamics are quantified using an
17 analytical model.

18 2. The strongest impacts occurred during autumn and winter due to the seasonal
19 freshwater regulation by TGD.

20 3. The alteration of tide-river dynamics may exert considerable impacts on sustainable
21 water resource management in dam-controlled estuaries.

22

23

24

25

26

27



28 **Abstract**

29 The Three Gorges Dam (TGD), located in the mainstream of the Yangtze River, is the
30 world's largest hydroelectric station in terms of installed power capacity. It was
31 demonstrated that the TGD had caused considerable modifications in the downstream
32 freshwater discharge due to its seasonal operation mode of multiple utilisation for flood
33 control, irrigation, and power generation. To understand the impacts of the freshwater
34 regulation of TGD, an analytical model is adopted to explore how the operation of TGD
35 may affect the spatial-temporal patterns of tide-river dynamics in the Yangtze River
36 estuary. We evaluated the effect of TGD by comparing the changes in major tide-river
37 dynamics in the post-TGD period (2003–2014) with those in the pre-TGD period
38 (1979–1984). The results indicate that the strongest impacts occurred during the autumn
39 and winter, corresponding to a substantial reduction in freshwater discharge during the
40 wet-to-dry transition period and slightly increased discharge during the dry season. The
41 underlying mechanism leading to changes in the tide-river dynamics lies in the
42 alteration of freshwater discharge, while the impact of geometric change is minimal.
43 Overall, the results suggest that the spatial-temporal patterns of tide-river dynamics is
44 sensible to the freshwater regulation of the TGD, to the extent that the ecosystem
45 function of the estuary may undergo profound disturbances. The results obtained from
46 this study can be used to set scientific guidelines for water resource management (e.g.
47 navigation, flood control, salt intrusion) in dam-controlled estuarine systems.

48 **Key words:** seasonal freshwater regulation, Three Gorges Dam, analytical model, tide-
49 river dynamics, Yangtze River estuary



50 **1. Introduction**

51 Estuaries are transition zones where river meets ocean (Savenije, 2012). Tide-river
52 interactions, a result of both hydrologic drivers and geomorphic constraints, are highly
53 dynamic in estuaries (Buschman et al., 2009; Sassi and Hoitink, 2013; Guo et al., 2015;
54 Cai et al., 2016; Hoitink and Jay, 2016; Hoitink et al., 2017). In natural conditions, they
55 usually experience a wide range of temporal variations, including spring-neap tidal
56 fluctuations as well as seasonal-varying discharges (e.g. Zhang et al., 2018). Human
57 intervention, such as dam construction in the upstream parts of the river and the growing
58 number of water conservancy projects being built along large rivers (such as freshwater
59 withdrawal), have caused seasonal changes in downstream freshwater discharge
60 delivery, leading to adjustments in the function of fluvial and estuarine hydrology (e.g.
61 Lu et al., 2011; Mei et al., 2015; Dai et al., 2017). Consequently, it is important to
62 understand the impacts of large-scale human intervention, which are relevant not only
63 to tide-river dynamics and riparian ecology but also to sustainable water resource
64 management in general, such as flood control, navigation, salt intrusion, and freshwater
65 withdrawal.

66
67 River discharge generally fluctuates following a wet-dry cycle due to the seasonal
68 variation of precipitation in the upstream river basin. For instance, the Yangtze River, a
69 large river, which flows into the East China Sea, has a maximum river discharge during
70 summer in July and a low value during winter in January, with a maximum discharge
71 difference of approximately 38,000 m³/s (Cai et al., 2016). Similar seasonal variations



72 are also identified in other large rivers in eastern and southern Asia, such as the Mekong
73 River in Vietnam, Ganges River in India, and Pearl River in China, under the influence
74 of a monsoon climate. However, most large rivers have been significantly dammed at
75 the central and upper reaches in recent decades, dramatically modifying stream
76 hydrology and sediment delivery, resulting in changes in hydraulics and river delta
77 development trend at the lower reaches (e.g. Räsänen et al, 2017; Rahman et al., 2018;
78 Liu et al., 2018). Due to the fact that the response of tide-river interactions to the
79 impacts of dams are diverse and non-uniform and that many more dams are to be built
80 in the future, the impacts of the hydrodynamic interactions between tidal waves and
81 seasonal river flows from natural variations and anthropogenic activities have become
82 a common focus in international hydraulic research, especially in large tidal rivers.

83

84 The Yangtze River estuary, located near the coastal area of East China Sea, is one of the
85 largest estuaries in Asia. In the mouth of the Yangtze River estuary, bifurcation occurs
86 and the characteristics of tides have been broadly investigated in previous studies (e.g.
87 Zhang et al., 2012; Lu et al., 2015; Alebregtse and Swart, 2016). However, in these
88 studies, river influences are usually neglected. In recent years, the processes of
89 nonlinear interactions between tidal wave and river flow in the Yangtze River estuary
90 have received increasing attention (e.g. Guo et al., 2015; Zhang et al., 2015a, b; Cai et
91 al., 2016; Kuang et al., 2017; Zhang et al., 2018). However, recent studies that have
92 been mainly concerned with tidal properties, such as asymmetry, changes near the
93 mouth area, and seasonal variations in tidal wave propagation and fluvial effects over



94 the entire 600 km of the tidal river, up to the tidal limit of the Datong hydrological
95 station, have been limited. In addition, the operation of the Three Gorges Dam (TGD),
96 the largest dam in the world, has substantially affected the downstream river hydrology
97 and sediment delivery. There is a variety of debate regarding the potential impacts of
98 TGD on the downstream river morphology, hydrology, and ecology, since the
99 underlying mechanism of the impact of the TGD is not fully understood. Specifically,
100 the TGD's operation has altered the downstream fluvial discharge and water levels on
101 the seasonal scale, directly following the reservoir seasonal impounding and release of
102 water volume (e.g. Chen et al., 2016; Guo et al., 2018). However, the impacts of
103 seasonal freshwater regulation by the TGD on the spatial-temporal tide-river dynamics
104 in the downstream estuarine area have not been systematically investigated. For
105 instance, during the dry season it was observed that the multi-year monthly averaged
106 river discharge at Datong hydrological station was altered from $9520 \text{ m}^3 \cdot \text{s}^{-1}$ to 12896
107 $\text{m}^3 \cdot \text{s}^{-1}$ in January due to the operation of the TGD, while during the wet season the river
108 discharge was altered from $49900 \text{ m}^3 \cdot \text{s}^{-1}$ to $44367 \text{ m}^3 \cdot \text{s}^{-1}$ in July owing to the TGD's
109 regulation.

110

111 In this study, for the first time, the spatial-temporal variations in the hydrodynamic
112 processes due to the interactions of tidal flow and fluvial discharge in the Yangtze River
113 estuary caused by natural forcing and human intervention were studied, with specific
114 focus on the TGD seasonal regulation effect. Here, we adopted a well-developed
115 analytical model proposed by Cai et al. (2014a, 2016) to investigate the spatial-temporal



116 patterns of tide-river dynamics in the entire Yangtze River estuary and quantify the
117 impacts of the TGD's operation. In the following sections, we introduce the study site
118 of the Yangtze River estuary. This is followed by a description of the available data and
119 analytical model of tide-river dynamics in Section 3. Subsequently, we apply the model
120 to the Yangtze River estuary, where the TGD has operated since 2003 (Section 4). In
121 particular, we explore the alteration of the tide-river dynamics after the TGD closure
122 and summarise the impacts of the TGD on the spatial-temporal patterns of tide-river
123 dynamics. The impacts of channel geometry and river discharge alterations on tide-river
124 dynamics as well as the implications for sustainable water resource management are
125 then discussed in Section 5. Finally, some key findings are addressed in Section 6.

126

127 **2. Overview of the Yangtze River estuary**

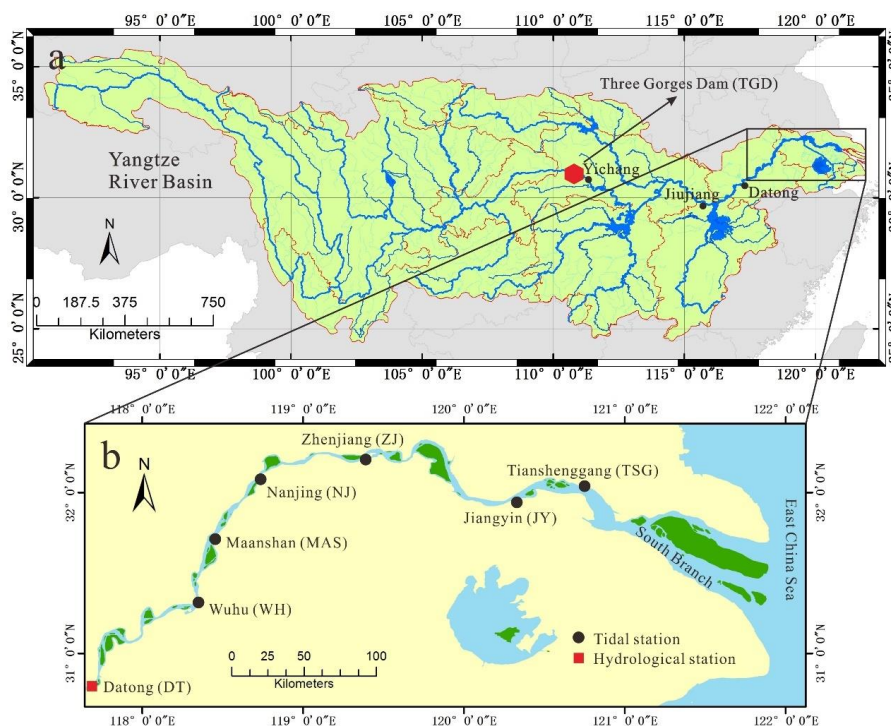
128 The Yangtze River, flowing from west to east in central China, is one of the world's
129 most important rivers due to its great economic and social relevance. It has a length of
130 about 6300 km and a basin area of about 190,000 km² (Figure 1a). The Yangtze River
131 basin is geographically divided into three parts, the upper, central, and lower sub-basins,
132 and contains an estuary area with partitions at Yichang, Jiujiang, and Datong (DT),
133 respectively (Figure 1a). Of concern in this study are the impacts of the Three Gorges
134 Dam (TGD), the world's largest dam, on the spatial-temporal patterns of tide-river
135 dynamics in the estuarine area. It is located about 45 km upstream of Yichang (Figure
136 1a). The TGD project began in 2003; by 2009, when full operations began, the total
137 water storage capacity rose up to ~40 km³, equivalent to 5% of the Yangtze's annual



138 discharge. Downstream of the DT station, where the tidal limit is located, the Yangtze
139 River estuary extends ~630 km to the seaward end of the South Branch. Wuhu (WH),
140 Maanshan (MAS), Nanjing (NJ), Zhenjiang (ZJ), Jiangyin (JY), and Tianshenggang
141 (TSG) are the major gauging stations along the mainstream in the seaward direction
142 (Figure 1b). Under the control of the Asian monsoon climate, river discharges show
143 distinct seasonal patterns. In 1979–2012, more than 70% of freshwater discharge at DT
144 occurred during summer (May–October).

145

146 Apart from river flows, tidal waves are also recognised as the major sources of energy
147 for hydrodynamics in the Yangtze River estuary, which is characterised by a meso-tide
148 with a tidal range that extends up to ~4.6 m and a mean tidal range of ~2.7 m near the
149 estuary mouth. According to the observation in the Gaoqiaoju tidal gauging station
150 (1950–2012), the averaged ebb tide duration (7.5 h) is a bit longer than the averaged
151 flood tide duration (5 h), indicating an irregular semidiurnal character (Zhang et al.,
152 2012). Unlike previous studies focusing on tidal hydrodynamics near the estuary mouth,
153 or water and sediment alterations since the beginning of TGD's operation, here, we
154 mainly concentrate on the tide-river dynamics under the impacts of TGD seasonal
155 regulation over the entire reach of the Yangtze River estuary.



156

157 Figure 1. Sketch maps of the Yangtze River basin (a) and Yangtze River estuary (b),

158 displaying the location of gauging and hydrological stations.

159

160 3. Data and Methodology

161 3.1 Source of Data

162 To quantitatively investigate the relationship between freshwater discharge regulation
163 caused by the TGD's operation and the tide-river dynamics, monthly averaged
164 hydrological data for both pre-TGD (1979–1984) and post-TGD (2003–2014) periods
165 of tidal range and water level from the above-mentioned six tidal gauging stations along
166 the Yangtze River estuary were collected. They were published by the Yangtze
167 Hydrology Bureau of the People's Republic of China. The monthly averaged tidal



168 amplitude is determined by averaging the daily difference of high and low water levels
169 and a half. To correctly quantify the residual water level along the Yangtze estuary,
170 locally measured water levels of different gauging stations are corrected to the national
171 mean sea level of Huanghai 1985.

172

173 **3.2 Analytical model for tide-river dynamics**

174 **3.2.1 Basic equations**

175 In tidal rivers, the tidally averaged water level (i.e. residual water level) depicts a steady
176 gradient, which usually increases with freshwater discharge (e.g. Sassi and Hoitink,
177 2013). The key to deriving the dynamics of the residual water level lies in the one-
178 dimensional momentum equation, which can be expressed as (e.g. Savenije, 2005,
179 2012):

$$180 \quad \frac{\partial U}{\partial t} + U \frac{\partial U}{\partial x} + g \frac{\partial Z}{\partial x} + \frac{gh}{2\rho} \frac{\partial \rho}{\partial x} + g \frac{U |U|}{K^2 h^{4/3}} = 0, \quad (1)$$

181 where U is the cross-sectional averaged velocity, Z is the free surface elevation, h is the
182 water depth, g is the acceleration due to gravity, t is the time, ρ is the water density, x is
183 the longitudinal coordinate directed landward, and K is the Manning-Strickler friction
184 coefficient. It was demonstrated that in the subtidal momentum balance, the residual
185 water level slope is primarily balanced by the residual friction term (Vignoli et al., 2003;
186 Buschman et al., 2009; Cai et al., 2014a, for a detailed derivation, readers can refer to
187 the Appendix A):

$$188 \quad \frac{\partial Z}{\partial x} = - \frac{U |U|}{K^2 h^{4/3}} \quad (2)$$

189



190 where the overbars indicate the tidal average. For a single channel with the residual
 191 water level set to 0 at the estuary mouth (i.e. $\bar{Z} = 0$ at $x = 0$), the integration of
 192 Equation (2) leads to an analytical expression for the residual water level

$$193 \quad \bar{Z}(x) = -\int_0^x \frac{\partial \bar{Z}}{\partial x} = -\int_0^x \frac{\overline{U|U|}}{K^2 h^{4/3}}. \quad (3)$$

194 To derive the analytical solutions for tide-river dynamics, we assume that the
 195 longitudinal variation of cross-sectional area \bar{A} and width \bar{B} can be described by the
 196 following exponential functions (see also Toffolon et al., 2006; Cai et al., 2014a):

$$197 \quad \bar{A} = \bar{A}_r + (\bar{A}_0 - \bar{A}_r) \exp\left(-\frac{x}{a}\right), \quad (4)$$

$$198 \quad \bar{B} = \bar{B}_r + (\bar{B}_0 - \bar{B}_r) \exp\left(-\frac{x}{b}\right), \quad (5)$$

199 where \bar{A}_0 and \bar{B}_0 represent the tidally averaged cross-sectional area and width at the
 200 estuary mouth, respectively, \bar{A}_r and \bar{B}_r represent the asymptotic riverine cross-
 201 sectional area and width, respectively, and a and b are the convergence lengths of the
 202 cross-sectional area and width, respectively. The advantage of these equations for
 203 approximating the shape of the estuary is that they account not only for the exponential
 204 shape in the lower part of the tidal river but also for the approximately prismatic channel
 205 in the upstream part of the tidal river. We further assume a nearly rectangular cross-
 206 section; hence, the tidally averaged depth is given by $\bar{h} = \bar{A}/\bar{B}$.

207 **3.2.2 Analytical solution for tidal hydrodynamics**

208 It was shown by Cai et al. (2014a, b, 2016) that the tide-river dynamics is dominantly
 209 controlled by four dimensionless parameters (see their definitions in Table 1). They
 210 include: the dimensionless tidal amplitude ζ (representing the boundary condition in the



211 seaward side), the estuary shape number γ (representing the cross-sectional area
 212 convergence), the friction number χ (representing the bottom frictional effect), and the
 213 dimensionless river discharge φ (representing the impact of freshwater discharge),
 214 where η is the tidal amplitude, v is the velocity amplitude, U_r is the river flow velocity,
 215 ω is the tidal frequency, r_s is the storage width ratio accounting for the effect of storage
 216 area (i.e. tidal flats or salt marshes), and c_0 is the classical wave celerity defined as
 217 $c_0 = \sqrt{g\bar{h}/r_s}$.

218 Table 1. Definitions of dimensionless parameters used in the analytical model

Local variables	Dependent variables
Dimensionless tidal amplitude $\zeta = \eta / \bar{h}$	Amplification number $\delta = c_0 d \eta / (\eta \omega d x)$
Estuary shape number $\gamma = c_0 (\bar{A} - \bar{A}_r) / (\omega a \bar{A})$	Velocity number $\mu = v / (r_s \zeta c_0) = v \bar{h} / (r_s \eta c_0)$
Friction number $\chi = r_s g c_0 \zeta [1 - (4\zeta / 3)^2]^{-1} / (\omega K^2 \bar{h}^{4/3})$	Celerity number $\lambda = c_0 / c$
Dimensionless river discharge $\varphi = U_r / v$	Phase lag $\varepsilon = \pi / 2 - (\phi_z - \phi_v)$

219

220 In this study, we used the analytical solutions proposed by Cai et al. (2014a, b, 2016),
 221 in which the solutions of the major tide-river dynamics are derived by solving a set of
 222 four implicit equations for the tidal damping, the velocity amplitude, the wave celerity,
 223 and the phase lag (see details in Appendix B). The major dependent parameters can be



224 described by the following four variables (see also Table 1): δ represents the
225 damping/amplification number describing the increase ($\delta > 0$), or decrease ($\delta < 0$) of
226 the tidal wave amplitude along the estuary axis, μ represents the velocity number
227 indicating the ratio of actual velocity amplitude to the frictionless value in a prismatic
228 channel, λ represents the celerity number representing the classical wave celerity c_0
229 scaled by the actual wave celerity c , and ε represents the phase lag between the high
230 water (HW) and high water slack (HWS) or between the low water (LW) and low water
231 slack (LWS). It is important to note that the phase lag (ranging between 0 and $\pi/2$) is a
232 key parameter in classifying the estuary, where $\varepsilon = 0$ suggests the tidal wave is featured
233 by a standing wave, while $\varepsilon = \pi/2$ indicates a progressive wave. For a simple harmonic
234 wave, the phase lag is defined as $\varepsilon = \pi/2 - (\phi_z - \phi_v)$, where ϕ_z and ϕ_v are the phases of
235 elevation and current, respectively (Savenije, et al., 2008).

236 3.2.3 Analytical solution for the entire channel

237 It is worth noting that the analytically computed tide-river dynamics μ , δ , λ , and ε only
238 represent local hydrodynamics since they depend on local (fixed position) values of the
239 dimensionless parameters, i.e. the tidal amplitude ζ , the estuary shape number γ , the
240 friction number χ , and the river discharge φ (see Table 1). To correctly reproduce the
241 tide-river dynamics for the entire channel, a multi-reach technique is adopted by
242 subdividing the entire estuary into multiple reaches to account for the longitudinal
243 variations of the estuarine sections (e.g. bed elevation, bottom friction). For a given
244 tidal damping/amplification number δ and tidal amplitude η at the seaward boundary, it
245 is possible to determine the tidal amplitude at a distance Δx (e.g. 1 km) upstream by



246 simple explicit integration. Hence, the analytical solution for the entire channel can be
247 obtained by step-wise integration in this way.

248

249 **4. Results**

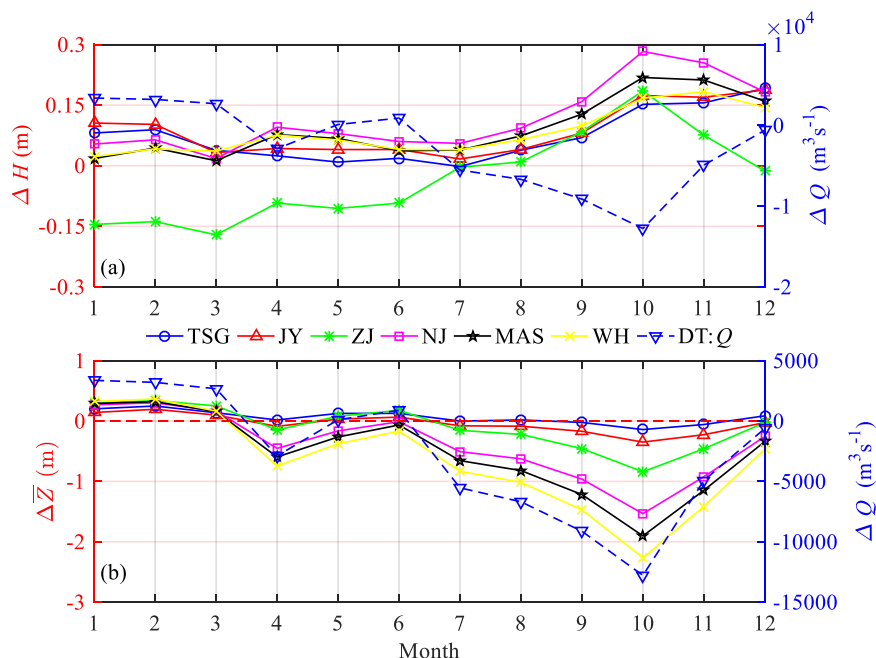
250 **4.1 Alteration of the tide-river dynamics after TGD closure**

251 To quantify the impacts of TGD's operation on the downstream tide-river dynamics,
252 we divided the time series into two periods, including a pre-TGD period (1979–1984,
253 representing the condition before the operation of the TGD) and a post-TGD period
254 (2003–2014, after the closure of the TGD with an operating TGD). Figure 2 shows the
255 changes in the observed tidal range ΔH and residual water level $\Delta \bar{Z}$ before and after
256 the closure of the TGD at the six gauging stations, together with the change in
257 freshwater discharge ΔQ observed at the DT hydrological station. Figure 2 and Table 2
258 clearly show that the monthly averaged river discharge in January, February, and March
259 substantially increased by 35.5%, 30.5%, and 16.4%, respectively, due to the
260 considerable release of freshwater from the TGD. On the other hand, we observe a
261 significant decrease in freshwater discharge in September, October, and November,
262 decreasing by 20.1%, 33.2%, and 20.8%, respectively. The reason can be primarily
263 attributed to the impounding water of the TGD during these months, especially in
264 October. During the other months, the impacts of TGD on the change in the freshwater
265 discharge are relatively small, mimicking the natural condition before the operation of
266 the TGD.

267



268 In Figure 2a we observe an increasing trend in tidal range for the post-TGD period at
269 the six gauging stations, except for the marked decrease at the ZJ station in the first half
270 of the year (i.e. January–June). On average, the maximum increase (0.20 m) in tidal
271 range occurs in October, which is mainly due to the substantial reduction of river
272 discharge caused by the TGD’s operation. This indicates a consistent enhancement of
273 tidal dynamics along the Yangtze estuary, except the reach near the ZJ station. For the
274 residual water level, Figure 2b clearly shows that the change in the residual water level
275 directly follows that of the river discharge due to the stable relationship between these
276 two parameters. In particular, we see that the residual water levels increased by 0.26 m,
277 0.30 m, and 0.16 m, respectively, in January, February, and March, while they
278 significantly decreased by 0.72 m, 1.17 m, and 0.70 m, respectively, in September,
279 October, and November. In addition, the decrease trend in residual water level is more
280 significant in upstream stations when compared with those in the downstream areas.



281

282 Figure 2. Changes in monthly averaged (a) tidal range ΔH and (b) residual water level

283 $\Delta \bar{Z}$ together with the freshwater discharge ΔQ along the Yangtze River estuary.

284

285 Table 2. Comparison of multi-year monthly averaged river discharge Q ($\text{m}^3 \cdot \text{s}^{-1}$)

286 between the pre-TGD and the post-TGD periods

Month	1	2	3	4	5	6	7	8	9	10	11	12
Pre-TGD	9520	10527	16298	25050	30867	38283	49900	47276	45317	38467	23633	14810
Post-TGD	12896	13733	18974	22165	30971	39180	44367	40590	36187	25682	18714	14203
Change	3376	3206	2675	-2885	105	896	-5533	-6687	-9130	-12784	-4919	-607

287

288 Since the TGD's operation affects tide-river dynamics primarily through the alteration

289 of the freshwater discharge, it is worth exploring the patterns of trends in the

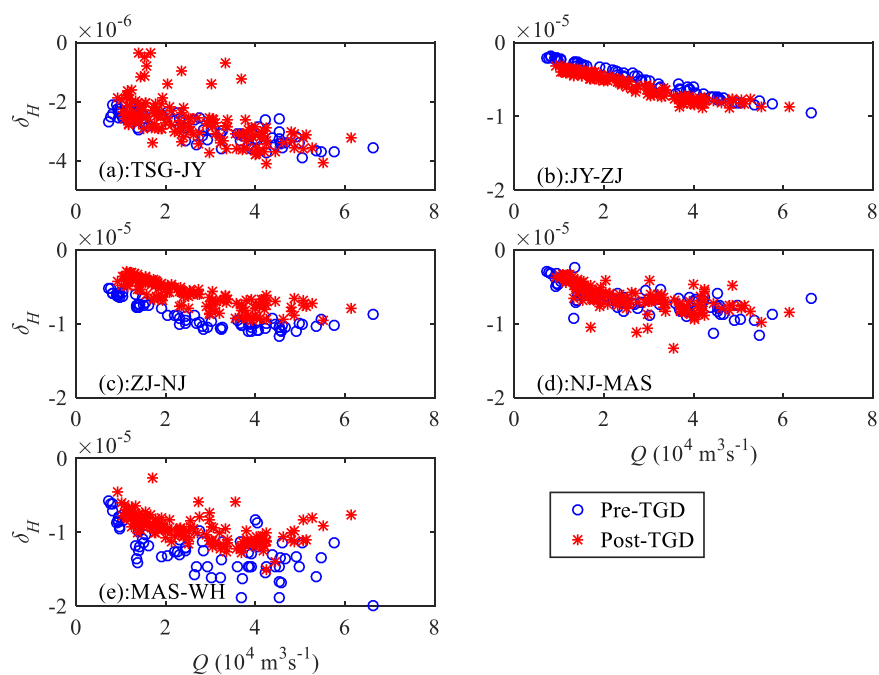


290 relationship between the freshwater discharge and gradients of the main tidal
291 parameters with respect to distance (i.e. the tidal damping rate and the residual water
292 level slope). Here, we estimated the tidal damping rate δ_H and the residual water level
293 slope S for a reach of Δx by using the following expressions:

$$294 \quad \delta_H = \frac{1}{(H_1 + H_2)/2} \frac{H_2 - H_1}{\Delta x}, \quad (6)$$

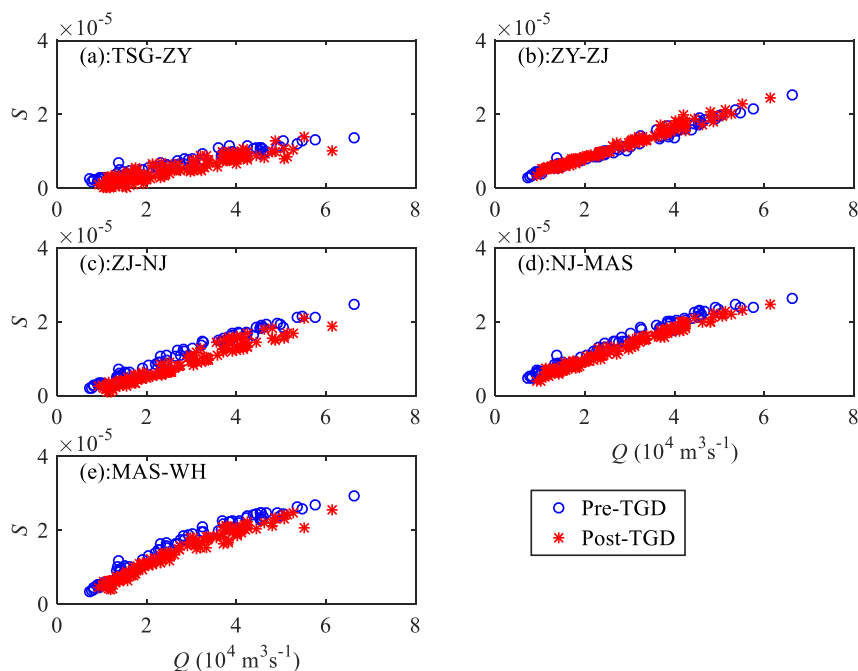
$$295 \quad S = \frac{\bar{Z}_2 - \bar{Z}_1}{\Delta x}, \quad (7)$$

296 where H_1 and \bar{Z}_1 are the tidal amplitude and residual water level on the seaward side,
297 respectively, whereas H_2 and \bar{Z}_2 are the corresponding values Δx upstream,
298 respectively. Figure 3 presents the computed tidal damping rates for different reaches
299 along the Yangtze estuary based on the observed tidal ranges at the six gauging stations.
300 It is remarkable that the tidal damping rates at the ZJ-NJ and MAS-WH reaches have
301 significantly increased during the post-TGD period, which suggests an enhancement of
302 tidal dynamics under the current freshwater discharge conditions. On the contrary, a
303 noticeable decrease in δ_H was observed at the JY-ZJ reach, which corresponds to a
304 decrease in tidal range at the ZJ station for the low river discharge conditions (from
305 January to May, see Figure 2a). At TGS-JY and NJ-MAS, no significant change in δ_H
306 is observed. In Figure 4, a consistent decrease in the residual water level slope S is
307 observed along the Yangtze estuary, except for the JY-ZJ reach. This means that the
308 residual friction effect becomes weaker in the post-TGD period since the residual water
309 level slope is primarily balanced by the residual friction term (Cai et al., 2014a, b, 2016).



310

311 Figure 3. Changes in tidal damping rate δ_H before and after the TGD closure for
312 different reaches along the Yangtze estuary: (a) TGS-JY, (b) JY-ZJ, (c) ZJ-NJ, (d) NJ-
313 MAS, (e) MAS-WH.



314

315 Figure 4. Changes in residual water level slope S before and after the TGD closure for
316 different reaches along the Yangtze estuary: (a) TGS-JY, (b) JY-ZJ, (c) ZJ-NJ, (d) NJ-
317 MAS, (e) MAS-WH.

318

319 4.2 Performance of the analytical model reproducing the tide-river dynamics

320 The analytical model presented in Section 3.2 was subsequently applied to the Yangtze
321 River estuary, with the seaward boundary using the tidal amplitude imposed at the TSG
322 station and the landward boundary using the river discharge imposed at the DT station.
323 The computation length of the estuary is 470 km, covering the entire estuary from TSG
324 to DT. The adopted geometric characteristics (including the tidally averaged cross-
325 sectional area, width, and depth) are the same for both pre- and post-TGD periods,
326 which were extracted from a digital elevation model (DEM) using Yangtze River

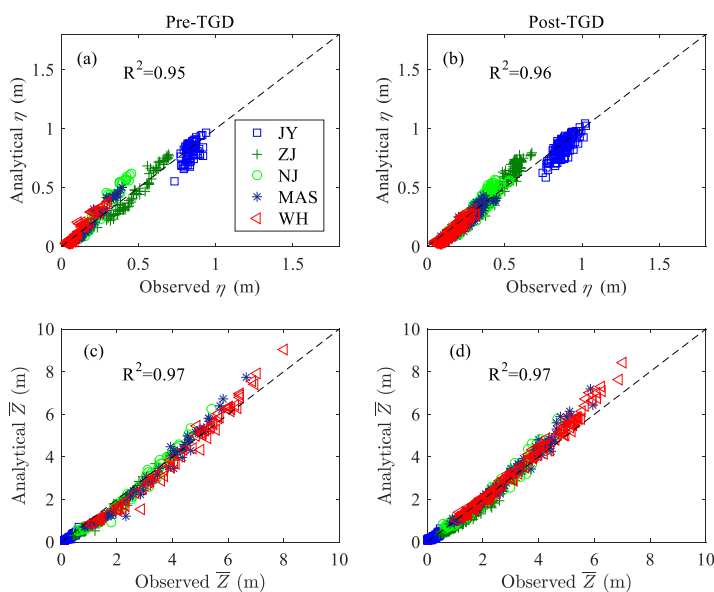


327 estuary navigation charts surveyed in 2007. The geometric characteristics, calibrated
 328 by fitting the observed values using Equations (4) and (5), are presented in Table 3,
 329 where a relatively large cross-sectional area convergence length ($a = 151$ km) is evident,
 330 with a relatively small width ($b = 44$ km), indicating a fast transition from a funnel-
 331 shaped reach to a prismatic reach in terms of width. It is worth noting that the Yangtze
 332 River estuary is characterised by a typical semidiurnal character; thus, a typical M_2 tidal
 333 period (i.e. 12.42 h) was adopted in the analytical model. For the sake of simplification,
 334 we assume that the storage width ratio $r_S = 1$. Hence, the only calibrated parameter is
 335 the Manning-Strickler friction coefficient K . Here, we used two values for K : $K = 80$
 336 $\text{m}^{1/3} \cdot \text{s}^{-1}$ in the tide-dominated region ($x = 0\text{--}42$ km), and a smaller value of $K = 55$
 337 $\text{m}^{1/3} \cdot \text{s}^{-1}$ in the river-dominated region ($x = 42\text{--}450$ km). The analytically computed
 338 results were compared with the observed tidal amplitudes and the residual water levels
 339 at five gauging stations along the Yangtze estuary (Figure 5). It can be seen that the
 340 overall correspondence between analytical results and observations is good, with high
 341 coefficients of determination ($R^2 > 0.95$), which suggests the usefulness of the present
 342 analytical model for reproducing the tide-river dynamics, given the gross features of
 343 flow characteristics and estuarine geometry.

344 Table 3. Characteristics of geometric parameters in the Yangtze River estuary

Characteristics	River	Mouth	Convergence length a/b (km)
Cross-sectional area \bar{A} (m^2)	12,135	51,776	151
Width \bar{B} (m)	2005	6735	44

345



346

347 Figure 5. Comparison of analytically computed tidal amplitude η (a, b) and residual
348 water level \bar{Z} (c, d) against the observations in the Yangtze River estuary for the pre-
349 TGD period (1979–1984) and post-TGD period (2003–2014).

350

351 **4.3 Impacts of TGD's operation on spatial-temporal patterns of tide-river** 352 **dynamics**

353 With the significant seasonal discharge variations resulting from the TGD regulation,
354 an understanding of the seasonal impacts on tide-river dynamics along the estuary has
355 become increasingly important. In Figures 6 and 7, we see how the TGD's operation
356 impacts the longitudinal variation of the main tidal dynamics in terms of the four
357 dependent parameters δ , λ , μ , and ε for different seasons. The most considerable changes
358 in the major tide-river dynamics occurred in both autumn and winter seasons, which
359 correspond to the substantial reduction in freshwater discharge in the wet-to-dry



360 transition period (i.e. autumn) and slightly increased freshwater discharge in the dry
361 season (i.e. winter) due to the TGD's operation since 2003 (see Table 2). On the other
362 hand, the impacts of the TGD's operation on the tide-river dynamics during the spring
363 and summer are relatively minor due to the negligible change in the freshwater
364 discharge. However, we do notice that the TGD had exerted slight influence on tide-
365 river dynamics in the downstream reaches ($x < 250$ km) during the summer, with the
366 maximum freshwater discharge occurring within a year. In addition, it appears that there
367 exists a critical position corresponding to the maximum tidal damping (or minimum
368 value of δ) upstream in which the tidal damping becomes weak. This phenomenon
369 occurs particularly in the spring, summer, and autumn. The underlying mechanism is
370 elaborated in the discussion section.

371

372 Figures 6a, c, e, g show the comparison of the analytically computed tidal damping
373 number δ before and after the closure of the TGD, in which we clearly identify that the
374 longitudinal tidal damping effect was considerably weakened in autumn, while it was
375 slightly enhanced in winter after the TGD closure. This was expected since freshwater
376 discharges tend to dampen the tidal wave primarily through the enhancement of the
377 friction term (Horrevoets et al., 2004; Cai et al., 2014a, b, 2016). Figures 6b, d, g, i
378 show a similar picture for the wave celerity number λ , which is positively correlated to
379 the tidal damping number δ , according to the celerity equation (11) in Appendix B.
380 Figure 7 shows the longitudinal computation of the velocity number μ and the phase
381 lag ε for both periods. The impacts of the TGD's operation on the velocity scale and

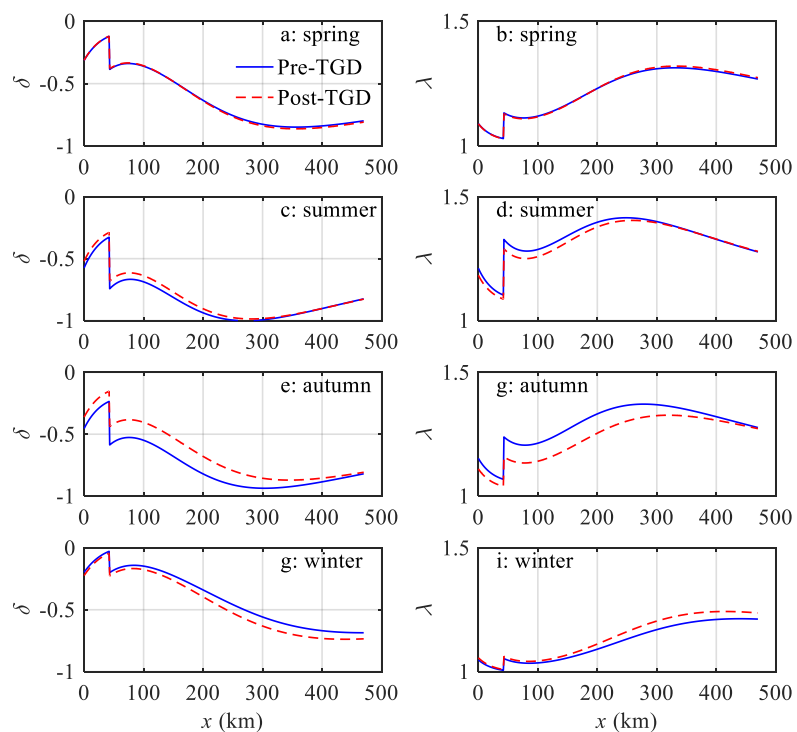


382 phase lag are similar to the tidal damping, i.e. the larger the freshwater discharge is, the
383 smaller the velocity number and the phase lag are.

384

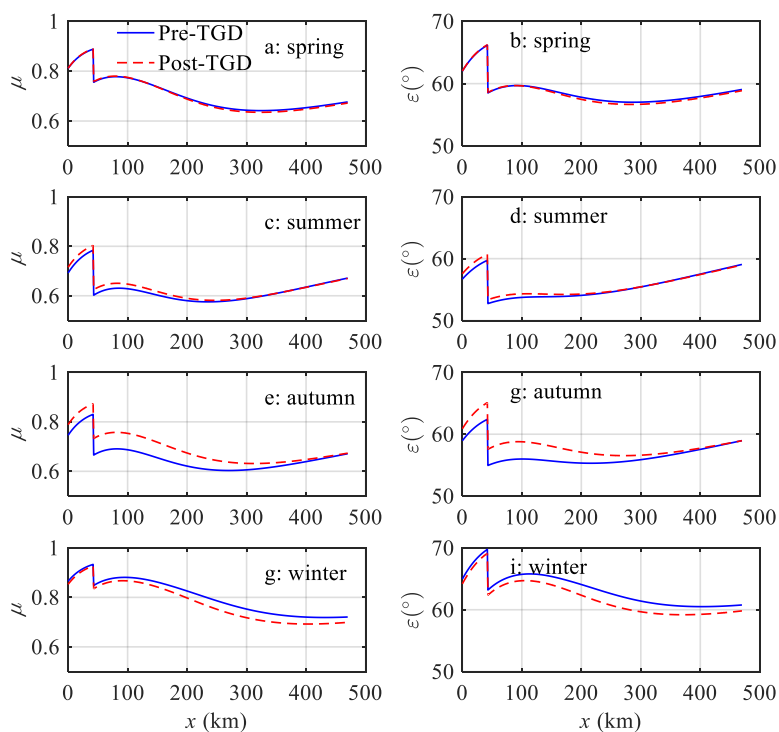
385 Overall, in the seaward reach of the estuary, the effect of freshwater discharge alteration
386 by the TGD's operation on the major tide-river dynamics (i.e. δ , λ , μ , and ε) was less
387 significant because of the small ratio of freshwater discharge to tidal discharge. On the
388 other hand, in the upstream reach of the estuary, the changes in the four dependent
389 parameters are also small due to the substantial tidal attenuation as a result of the long-
390 distance propagation from the estuary mouth. Therefore, the pattern of seasonal
391 variation due to the TGD's operation is relatively small at both ends of the estuary,
392 whereas the largest variation usually occurs in the middle reach of the estuary. This
393 finding was supported by the results of harmonic analysis using the numerical results
394 (Zhang et al., 2018). Similar phenomena have also been identified in other large fluvial
395 meso-tide estuaries, such as the Mekong River estuary and Amazon River estuary,
396 where dam operation altered the seasonal patterns of tide-river dynamics (Kosuth et al.,
397 2009; Hecht et al., 2018).

398



399

400 Figure 6. Longitudinal variability of simulated tidal damping number δ (a, c, e, g) and
401 celerity number λ (b, d, g, i) along the Yangtze estuary in different seasons (spring: a,
402 b; summer: c, d; autumn: e, g; winter: g, i) for both the pre-TGD and the post-TGD
403 periods.



404

405 Figure 7. Longitudinal variability of simulated velocity number μ (a, c, e, g) and phase
406 lag ε (b, d, g, i) along the Yangtze estuary in different seasons (spring: a, b; summer: c,
407 d; autumn: e, g; winter: g, i) for both the pre-TGD and the post-TGD periods.

408

409 5. Discussion

410 5.1 The impact of channel geometry alteration on tide-river dynamics

411 Dam operations, which dramatically modified downstream flow and sediment regimes,
412 are becoming an increasingly important factor controlling the morphological evolution.

413 Previous studies show that, as a result of the trapping of sediments by the TGD,
414 considerable erosion occurred in the first several hundred km downstream of the TGD,



415 considerably coarsening the bedload (Yang et al., 2014). In particular, the river
416 immediately downstream eroded at a rate of 65 Mt/yr in 2001–2002 (Yang et al., 2014).
417 It was shown by Lyu et al. (2018) that due to a dramatic reduction in the sediment
418 discharge following the construction of the TGD, a significant change in size, geometry,
419 and spatial distribution of pool-riffles occurred downstream; however, this adjustment
420 was limited to the reaches close to the TGD. It should be noted that the bathymetry
421 adopted in the analytical model is restricted to the estuarine area in 2007, which is only
422 4 years after the TGD closure in 2003, and it is before the full operation of the TGD
423 began in 2009. In addition, the TGD is around 1600 km away from the estuary mouth,
424 and its influence on the estuarine morphology normally has a lag effect of at least 4–5
425 years, as discussed by Wang et al. (2008). Hence, the adopted geometry has been only
426 partly altered after the TGD closure. Consequently, we concluded that the impact of the
427 channel geometry alteration on tide-river dynamics in the Yangtze River estuary is
428 limited and, thus, the correspondence with the observed tidal amplitude and residual
429 water level for the pre-TGD period is good, such that we even used the geometry
430 surveyed in 2007.

431 **5.2 The impact of freshwater discharge alteration on tide-river dynamics**

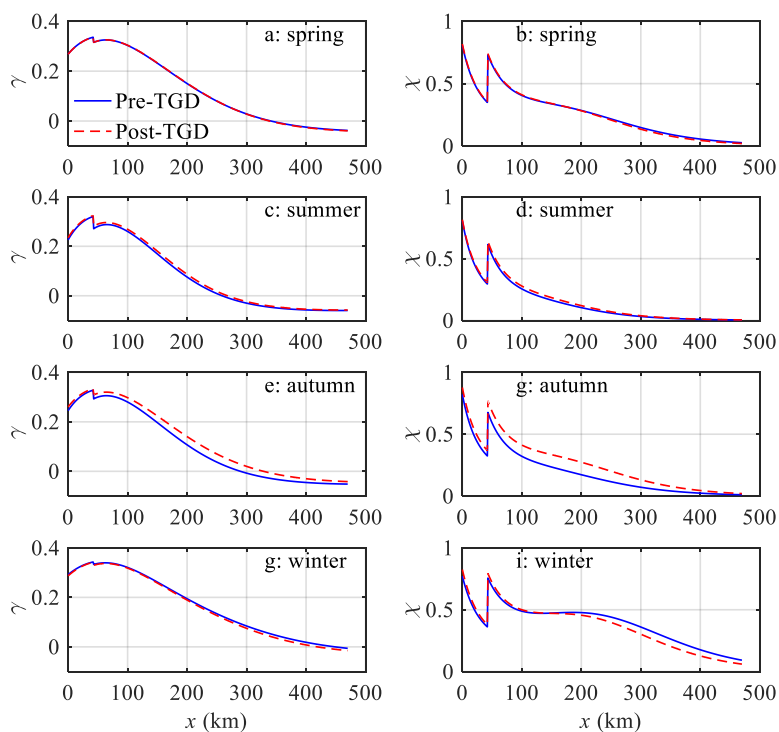
432

433 The water conservancy of the TGD has multiple purposes, in which the seasonal
434 discharge regulation and their impact on the ecosystem are well documented (e.g. Mei
435 et al., 2015a, b; Chen et al., 2016; Guo et al., 2018). However, the actual influence of
436 discharge regulation on the river-tide dynamics in the estuarine area is not fully



437 understood. With the analytical reproduction of tide-river dynamics for pre- and post-
438 TGD periods, it is possible to quantify the extent of the changes in the major tidal
439 dynamics, including the estuary shape number γ and friction number χ (Figure 8), and
440 the residual water level slope S and water depth h (Figure 9) along the Yangtze River
441 estuary. In general, during the transition from the wet season (summer–autumn) to the
442 dry season (winter–spring), the water level and corresponding fluvial discharge
443 downstream from the TGD is first raised by the impounding water and then reduced by
444 the release of water, which would substantially change the tide-river dynamics in the
445 downstream estuarine area, with the maximum variation occurring in autumn and the
446 minimum variation occurring in spring.

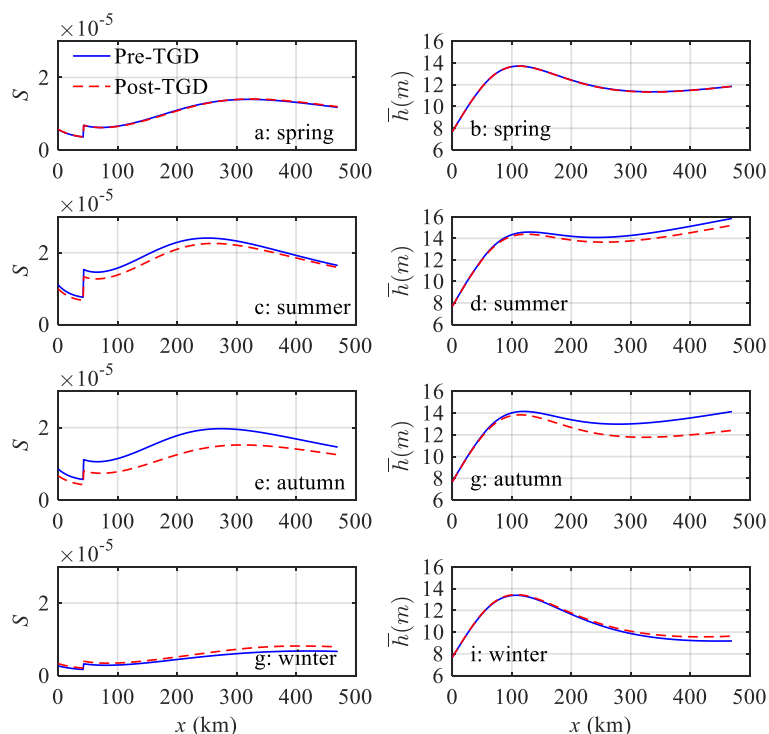
447



448

449 Figure 8. Longitudinal variability of simulated estuary shape number γ (a, c, e, g) and
450 friction number χ (b, d, g, i) along the Yangtze estuary in different seasons (spring: a, b;
451 summer: c, d; autumn: e, g; winter: g, i) for both the pre-TGD and the post-TGD periods.

452



453
 454 Figure 9. Longitudinal variability of simulated residual water level slope S (a, c, e, g)
 455 and water depth \bar{h} (b, d, g, i) along the Yangtze estuary in different seasons (spring: a,
 456 b; summer: c, d; autumn: e, g; winter: g, i) for both the pre-TGD and the post-TGD
 457 periods.

458
 459 Figures 8 and 9 show that during the wet season (summer–autumn), the estuary shape
 460 number γ and friction number χ experience a general increase, while a decrease in the
 461 residual water level slope S and water depth \bar{h} can be identified in the post-TGD
 462 period due to the reduction in freshwater discharge. However, the changes in these
 463 major dynamics vary significantly along the channel. Near the estuary mouth, where



464 the tidal influence dominates that of the freshwater discharge, the difference is
465 relatively small, as the magnitude of the freshwater discharge is small when compared
466 with that of the tidal discharge. Meanwhile at the upstream reach of the estuary, where
467 the riverine influence dominates that of the tide, the difference is also small due to the
468 attenuation of the tidal wave propagation over a long distance. Consequently, the most
469 significant changes in major tide-river dynamics occurred in the middle reach of the
470 Yangtze River estuary due to the discharge regulation of the TGD during the wet season.
471 By contrast, during the dry season (winter–spring), especially in winter, the opposite
472 trend was observed, indicating a slight increase in γ and χ , and a slight decrease in S
473 and \bar{h} due to the additional release of discharge from the TGD. In addition, we also
474 observed that the changes in tide-river dynamics caused by the TGD's operation were
475 much stronger upstream than in the lower stream.

476

477 **5.3 Implications for water resource management**

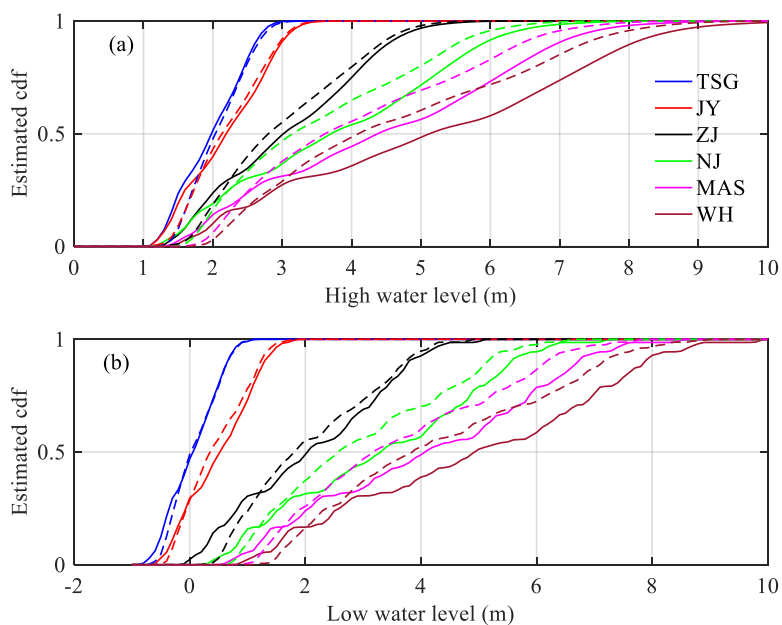
478 The construction of the TGD is the largest hydro-development project ever performed
479 in the world, having multiple influences on downstream water resource management,
480 including navigation, flood control, tidal limit variation, and salt intrusion.

481 **5.3.1 Implications for navigation**

482 The navigation condition is mainly controlled by both high water and low water levels.
483 Figure 10 shows the estimation of the cumulative distribution function (cdf) for both
484 the high-water level (Figure 10a) and the low-water level (Figure 10b) at the six
485 gauging stations along the Yangtze River estuary for both the pre- and post-TGD



486 periods. The results indicate that navigation conditions during the non-flood season are
487 generally improved, because both percentages of high-water and low-water levels are
488 increased due to the additional freshwater discharge released from the TGD. On the
489 other hand, during the flood season, the reduction in the freshwater discharge by TGD
490 impounding tends to exert a negative impact on navigation. However, the reduced
491 freshwater discharges in the late summer and autumn are not of sufficient magnitude to
492 cause any navigation problems. This is due to the fact that the mean water levels during
493 the flood season are relatively high; hence, the regulating flow quantity and regulating
494 capacity are relatively small (e.g. Chen et al., 2016). In general, due to the staggered
495 regulation in freshwater discharge, seasonally, the actual navigation condition is
496 improved due to the significant increase in the percentage of low water levels.



497

498 Figure 10. Cumulative distribution function (cdf) estimated by using the kernel



499 smoothing function for high water level (a) and low water level (b) at six gauging
500 stations along the Yangtze estuary. The drawn lines represent the pre-TGD period, while
501 the dashed lines represent the post-TGD period.

502 **5.3.2 Implications for flood control**

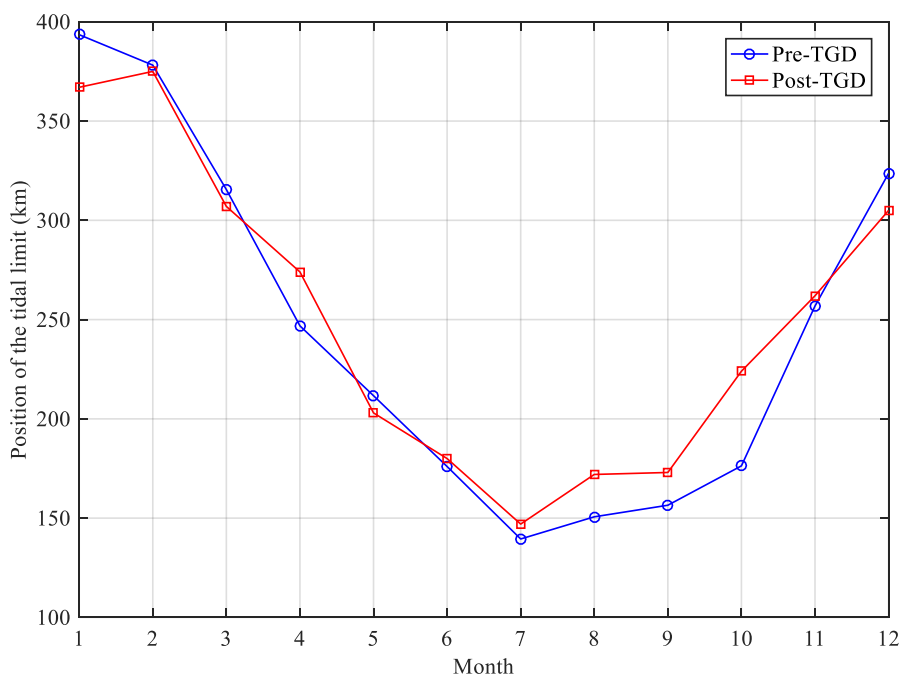
503 Flood control is one of the most important functions of building dams and reservoirs in
504 large rivers. Before the construction of the TGD, the Yangtze River basin suffered from
505 frequent and disastrous flood threats. For instance, the floods of 1998 in the Yangtze
506 River were reported to have killed 3656 people, destroyed 5.7 million homes, and
507 damaged seven million more. Many studies have examined the flood control capacity
508 of the TGD over the past two decades (Zhao et al., 2013; Chen et al., 2014). In particular,
509 the capability of the TGD flood control is influenced by multiple factors (e.g. Huang et
510 al., 2018), particularly in the estuarine area, which is strongly influenced by tides from
511 the ocean. During the flood season, the reduced freshwater discharge by TGD
512 impounding benefits the flood control by reducing the peak flood discharge. However,
513 as the tidal influence is enhanced, both the percentages of high water and low water
514 levels for the post-TGD period are considerably increased, as shown in Figure 10,
515 indicating a decreased flood control capability. For instance, at the WH gauging station
516 located in the upstream part of the Yangtze River estuary, the 8-m high-water level
517 increased by approximately 10% after the TGD closure during the wet season. The
518 corresponding flood prevention standard, therefore, is reduced from the 20-year return
519 period to the 10-year return period due to the increased high-water level.

520 **5.3.3 Implications for tidal limit**

521 It is important to detect the position of the tidal limit (corresponding with the position
522 where the tidal amplitude to depth ratio is less than a certain threshold, e.g. $\frac{\eta}{h} < 0.02$),



523 which is the farthest point upstream where a river is affected by tidal fluctuations, since
524 it is essential for surveying, navigation, and fisheries management, in general (e.g. Shi
525 et al., 2018). Subsequently, we are able to define the tide-influenced length as the
526 distance upstream from the estuary mouth to the tidal limit. Generally, the tidal limit
527 fluctuates with the changes in the seasonal freshwater discharges. Field measurements
528 have demonstrated that tidal limit can reach as far as the NJ station and further upstream
529 during the dry season, while during the wet season, it is pushed down to the ZJ station
530 and may be pushed further downward to the JY station under spate conditions. Figure
531 11 shows the analytically computed tidal limit position for both the pre- and post-TGD
532 periods. It can be observed that the tidal limit moved downstream by about 25 km and
533 250 km in January and December under the impact of the additional release of discharge
534 from TGD during the dry season. During the transition from dry to wet seasons
535 (January–May), the total freshwater discharge from TGD increases, and we identify
536 further downstream movement of the tidal limit, although to a smaller extent. The
537 reverse of the post-TGD tidal limit in April is due to the decrease in the freshwater
538 discharge compared with the pre-TGD tidal limit (see Table 2). The TGD storage period
539 begins in June, and the tidal limit moved upstream by a large amount compared with
540 the pre-TGD period. The largest change occurred during October when the tidal limit
541 moved from 175 km pre-TGD to 225 km post-TGD due to the substantial increase in
542 freshwater discharge (see Table 2).



543

544 Figure 11. Temporal variation of the position of the tidal limit relative to the TSG station
545 for both the pre-TGD and the post-TGD periods.

546 5.3.4 Implications for salt intrusion

547 The operation of the TGD changed the location of tidal limit, which, in turn, directly
548 influences the intensity of saltwater intrusion, especially during the dry season, when
549 the freshwater discharge is low and saltwater intrusion is important (e.g. Cai et al.,
550 2015). The analysis of tide-river dynamics shows that the tidal dynamics are
551 considerably enhanced during the autumn due to the substantial decline in freshwater
552 discharged into the estuary, which may lead to enhanced saltwater intrusion. However,
553 with supplemented discharge after the TGD during the winter, saltwater intrusion tends
554 to be significantly suppressed, and the isohalines are pushed seaward by additional river
555 discharges (e.g. An et al., 2009; Qiu and Zhu, 2013). In contrast, during the wet season,



556 the TGD's operation slightly extended the timing of saltwater intrusion and increased
557 its intensity by impounding freshwater. Since the total river discharge rate during the
558 wet season is the largest during the year, the influence of saltwater on freshwater
559 reservoirs along the coastal area is limited. Therefore, the operation of TGD is overall
560 favourable for reducing the burden of freshwater supplement in the tidally influenced
561 estuarine areas.

562 **6. Conclusions**

563 An analytical approach was used to examine the potential impacts of TGD's operation
564 on the spatial-temporal patterns of tide-river dynamics along the Yangtze River estuary.
565 It was shown that the freshwater regulation caused by the TGD, on a seasonal scale,
566 exerts significant impacts on the tide-river dynamics, with the maximum influence
567 occurring in autumn and winter. This generally corresponds to a dramatic decrease in
568 freshwater discharge during the wet-to-dry transition period and a slight increase in
569 discharge during the dry season. The analytical results indicate that the discharge
570 regulation by the TGD drives the alterations in the tide-river dynamics instead of the
571 geometric change. In particular, the change in the freshwater discharge changes the
572 estuary shape number (representing the geometric effect), the residual water level slope
573 (representing the effective frictional effect) and, hence, the tide-river dynamics. This
574 study, using the Yangtze River estuary as a significant case study, provides an effective
575 yet simple method to quantify the seasonal regulation in freshwater discharge by large
576 reservoirs or dams on hydrodynamics in estuaries. The results obtained from this study
577 will, hopefully, shed new light on aspects of water resource management, such as



578 navigation, flood control, and salt intrusion.

579

580 **Acknowledgments**

581 We acknowledge the financial support from the Open Research Fund of State Key
582 Laboratory of Estuarine and Coastal Research (Grant No. SKLEC-KF201809), from
583 the National Natural Science Foundation of China (Grant No. 51709287 and 41701001),
584 from the Basic Research Program of Sun Yat-Sen University (Grant No. 17lgzd12), and
585 from the Guangdong Provincial Natural Science Foundation of China (Grant No.
586 2017A030310321).

587

588

589 **References**

590 An, Q., Wu., Y., and Taylor, S., 2009. Influence of the Three Gorges Project on saltwater
591 intrusion in the Yangtze River Estuary. *Environ. Geol.*, 56, 1679-1686.

592 Alebregtse, N. C., and de Swart, H. E., 2016. Effect of river discharge and geometry on
593 tides and net water transport in an estuarine network, an idealized model applied to the
594 Yangtze estuary, *Cont. Shelf. Res.*, 123, 29-49.

595 Buschman, F. A., Hoitink, A. J. F., van der Vegt, M., and Hoekstra, P., 2009. Subtidal
596 water level variation controlled by river flow and tides, *Water Resour. Res.*, 45(10),
597 W10420.

598 Cai, H., Savenije, H. H. G., and Toffolon, M., 2014a. Linking the river to the estuary,
599 influence of river discharge on tidal damping, *Hydrol. Earth Syst. Sci.*, 18(1), 287-304.



- 600 Cai, H., Savenije, H. H. G., and Jiang, C., 2014b. Analytical approach for predicting
601 fresh water discharge in an estuary based on tidal water level observations, *Hydrol.*
602 *Earth Syst. Sci.*, 18(10), 4153-4168.
- 603 Cai, H., Savenije, H.H.G., Zuo, S., Jiang, C., and Chua, V., 2015. A predictive model
604 for salt intrusion in estuaries applied to the Yangtze estuary, *J. Hydrol.*, 529, 1336-1349.
- 605 Chen, J., Finlayson, B.L., Wei, T., Sun, Q., Webber, M., Li, M., and Chen, Z, 2016.
606 Changes in monthly flows in the Yangtze River, China-With special reference to the
607 Three Gorges Dam. *Journal of Hydrology*, 536, 293-301.
- 608 Chen, J., Zhong, P.A., Zhao, Y.F., 2014. Research on a layered coupling optimal
609 operation model of the three gorges and gezhouba cascade hydropower stations. *Energy*
610 *Convers. Manage.* 86 (5), 756–763.
- 611 Dai, M., Wang, J., Zhang, M., and Chen, X., 2017. Impact of the Three Gorges Project
612 operation on the water exchange between Dongting Lake and the Yangtze River, 32,
613 506-514.
- 614 Dronkers, J. J., 1964. *Tidal Computations in River and Coastal Waters*, Elsevier, New
615 York.
- 616 Friedrichs, C. T., and Aubrey, D. G., 1988. Non-linear tidal distortion in shallow well-
617 mixed estuaries, A synthesis, *Estuarine Coastal& Shelf Sci.*, 27, 521-545.
- 618 Guo, L., van der Wegen, M., Jay, D.A., Matte, P., Wang, Z.B., Roelvink, D.J.A., He, Q.,
619 2015. River-tide dynamics, Exploration of nonstationary and nonlinear tidal behavior
620 in the Yangtze River estuary. *J. Geophys. Res.*, 120(5), 3499-3521.
- 621 Guo, L., Su, N., Zhu, C., and He, Q., 2018. How have the river discharges and sediment



622 loads changed in the Changjiang River basin downstream of the Three Gorges Dam?
623 Journal of Hydrology, 560, 259-274.

624 Hoitink, A. J. F., and Jay, D. A., 2016. Tidal river dynamics, implications for deltas.
625 Rev. Geophys., 54, 240-272.

626 Hoitink, A. J. F., Wang, Z. B., Vermeulen, B., Huismans, Y., and Kastner, K., 2017. Tidal
627 controls on river delta morphology, Nat. Geosci., 10.

628 Horrevoets, A. C., Savenije, H. H. G., Schuurman, J. N., and Graas, S., 2004. The
629 influence of river discharge on tidal damping in alluvial estuaries, J. Hydrol., 294, 213-
630 228.

631 Hecht, J.S., Lacombe, G., Arias, M.E., Duc Dang, T. and Piman, T., 2018. Hydropower
632 dams of the Mekong River basin, a review of their hydrological impacts. Journal of
633 Hydrology, 45(10): W10420.

634 Huang, K., Ye, L., Chen, L., Wang, Q., Dai, L., Zhou, J., Singh, V. P., Huang, M., and
635 Zhang, J., 2018. Risk analysis of flood control reservoir operation considering multiple
636 uncertainties, Journal of Hydrology, 565, 672-684.

637 Kuang, C., Chen, W., Gu, J., Su, T. C., Song, H., Ma, Y., and Dong, Z., 2017. River
638 discharge contribution to sea-level rise in the Yangtze River Estuary, China. Cont. Shelf.
639 Res., 134, 63-75.

640 Kosuth, P. et al., 2009. Sea-tide effects on flows in the lower reaches of the Amazon
641 River. ID - 20093321193. Hydrological Processes, 23(22), 3141-3150.

642 Lu, S., Tong, C., Lee, D.Y., Zheng, J., Shen, J., Zhang, W., and Yan, Y. 2015.
643 Propagation of tidal waves up in Yangtze Estuary during the dry season. Journal of



- 644 Geophysical Research Oceans 120(9): 6445-6473.
- 645 Lu, X.X., Yang, X., and Li, S. 2011. Dam not sole cause of Chinese drought. NATURE
646 475(7355): 174.
- 647 Lyu, Y., Zheng, S., Tan, G. and Shu, C., 2018. Effects of Three Gorges Dam operation
648 on spatial distribution and evolution of channel thalweg in the Yichang-Chenglingji
649 Reach of the Middle Yangtze River, China. Journal of Hydrology, 565, 429-442.
- 650 Mei, X., Dai, Z., Gelder, P.H.A.J. and Gao, J., 2015a. Linking Three Gorges Dam and
651 downstream hydrological regimes along the Yangtze River, China. Earth and Space
652 Science, 2(4), 94-106.
- 653 Mei, X., Dai, Z., Du, J. and Chen, J., 2015b. Linkage between Three Gorges Dam
654 impacts and the dramatic recessions in China's largest freshwater lake, Poyang Lake.
655 Scientific Reports, 5,18197.
- 656 Liu, F., Hu, S., Guo, X., Cai, H., Yang, Q., 2018. Recent changes in the sediment regime
657 of the Pearl River (South China), Causes and implications for the Pearl River Delta,
658 Hydrological Processes.
- 659 Qiu, C. and Zhu., J., 2013. Influence of seasonal runoff regulation by the Three Gorges
660 Reservoir on saltwater intrusion in the Changjiang River Estuary. Continental Shelf
661 Research, 71, 16-26.
- 662 Rahman, M., Dustegir, M., Karim, R., Haque, A., Nicholls, R. J., Darby, S. E.,
663 Nakagawa, H., Hossain, M., Dunn, F. E., and Akter, M., 2018. Recent sediment flux to
664 the Ganges-Brahmaputra-Meghna delta system, Science of The Total Environment, 643,
665 1054-1064.



- 666 Räsänen, T. A., Someth, P., Lauri, H., Koponen, J., Sarkkula, J., and Kummu, M., 2017.
667 Observed river discharge changes due to hydropower operations in the Upper Mekong
668 Basin, *Journal of Hydrology*, 545, 28-41.
- 669 Sassi, M. G., and Hoitink, A. J. F., 2013. River flow controls on tides and tide-mean
670 water level profiles in a tidal freshwater river, *J. Geophys. Res.*, 118(9), 4139-4151.
- 671 Savenije, H. H. G., 2005. *Salinity and Tides in Alluvial Estuaries*, Elsevier, New York.
- 672 Savenije, H. H. G., 2012. *Salinity and Tides in Alluvial Estuaries* (2nd completely
673 revised edition), Available at www.salinityandtides.com.
- 674 Savenije, H. H. G., Toffolon, M., Haas, J., and Veling, E. J. M., 2008. Analytical
675 description of tidal dynamics in convergent estuaries, *J. Geophys. Res.*, 113, C10025.
- 676 Shi, S., Cheng, H., Xuan, X., Hu, F., Yuan, X., Jiang, Y., and Zhou, Q., 2018.
677 Fluctuations in the tidal limit of the Yangtze River estuary in the last decade, *Science*
678 *China Earth Sciences*, 61 (8) :1136-1147.
- 679 Wang, Y., Ridd, P.V., Wu, H., Wu, J. and Shen, H., 2008. Long-term morphodynamic
680 evolution and the equilibrium mechanism of a flood channel in the Yangtze Estuary
681 (China). *Geomorphology*, 99(1-4), 130-138.
- 682 Vignoli, G., Toffolon, M., and Tubino, M., 2003. Non-linear frictional residual effects
683 on tide propagation, in, *Proceedings of XXX IAHR Congress*, vol. A, 24-29 August
684 2003, Thessaloniki, Greece, 291-298.
- 685 Zhang, E. F., Savenije, H. H. G., Chen, S. L., and Mao, X. H., 2012. An analytical
686 solution for tidal propagation in the Yangtze Estuary, China, *Hydrol. Earth Syst. Sci.*,
687 16(9), 3327-3339.



688 Zhang, F., Sun, J., Lin, B., and Huang, G., 2018. Seasonal hydrodynamic interactions
689 between tidal waves and river flows in the Yangtze Estuary, *J. Marine Syst.*, 186, 17-
690 28.

691 Zhang, M., Townend, I., Cai, H., and Zhou, Y., 2015a. Seasonal variation of tidal prism
692 and energy in the Changjiang River estuary, A numerical study, *Chinese Journal of*
693 *Oceanology and Limnology*, 34 (1) :1-12.

694 Zhang, M., Townend, I., Cai, H., and Zhou, Y., 2015b. Seasonal variation of river and
695 tide energy in the Yangtze estuary, China, *Earth Surf. Process. and Landforms*, 41(1):
696 98-116.

697 Zhao, T., Zhao, J., Yang, D. and Wang, H., 2013. Generalized martingale model of the
698 uncertainty evolution of streamflow forecasts, *Adv. Water Resour.*, 57, 41-51.

699

700 **Appendix A. Simplified momentum balance for the residual water level slope**

701 Assuming a periodic variation of flow velocity, the integration of Equation (1) over a
702 tidal cycle leads to an expression for the residual water level slope (e.g. Cai et al., 2014a,
703 2016):

$$704 \quad \frac{\partial \bar{Z}}{\partial x} = -\frac{1}{K^2} \overline{\left(\frac{U|U|}{h^{4/3}} \right)} - \frac{1}{2g} \frac{\partial \bar{U}^2}{\partial x} - \frac{1}{2\rho_0} h \frac{\partial \bar{\rho}}{\partial x} \quad (8)$$

705 where the overbars and the subscript 0 indicate the tidal average and value at the
706 seaward boundary, respectively. The residual water level slope is induced by three
707 contributions: residual frictional, advective acceleration, and density effects, which
708 correspond to the three terms on the right-hand side of Equation (8). Note that the
709 contribution from advective acceleration to the residual water level slope:



$$710 \quad \frac{\partial \bar{Z}_{adv}}{\partial x} = -\frac{1}{2g} \frac{\partial \bar{U}^2}{\partial x}, \quad (9)$$

711 can be easily integrated to:

$$712 \quad \bar{Z}_{adv} = -\frac{1}{2g} (\bar{U}^2 - U_0^2) = -\frac{1}{2} \bar{Fr}_0 \left(\frac{\bar{U}^2}{U_0^2} - 1 \right) \bar{h}_0 \quad (10)$$

713 where the Froude number is introduced, $\bar{Fr}^2 = \bar{U}^2 / (g\bar{h})$, which is computed with the
 714 averaged variables. In this case, the correction is local (not cumulative) and
 715 proportional to the flow depth through a coefficient that is negligible as long as the
 716 velocity does not change significantly, and Fr is small, as is common in most tidal flows.
 717 It was shown by Savenije (2005, 2012) that the density term in equation (1) always
 718 exercises a pressure in the landward direction, which is counteracted by a residual water
 719 level slope, amounting to 1.25% of the estuary depth over the salt intrusion length. The
 720 value for the residual water level slope, induced by the density effect, is usually small
 721 compared with the gradient of the free surface elevation; thus, in this paper, we neglect
 722 the influence of the density difference on the dynamics of the residual water level.

723

724 **Appendix B. Governing equations for tide-river dynamics in estuaries**

725 The analytical solutions for the dependent parameters μ , δ , λ , and ε are obtained by
 726 solving the following four dimensionless equations (see details in Cai et al., 2014a):
 727 the tidal damping/amplification equation, describing the tidal amplification or damping
 728 as a result of the balance between channel convergence (gq) and bottom friction
 729 (cm/G):

$$730 \quad \delta = \frac{\mu^2 (\gamma\theta - \chi\mu\lambda\Gamma)}{1 + \mu^2\beta}, \quad (11)$$



731 the scaling equation, describing how the ratio of velocity amplitude to tidal amplitude
732 depends on phase lag and wave celerity:

$$733 \quad \mu = \frac{\sin(\varepsilon)}{\lambda} = \frac{\cos(\varepsilon)}{\gamma - \delta}, \quad (12)$$

734 the celerity equation, describing how the wave celerity depends on the balance between
735 convergence and tidal damping/amplification:

$$736 \quad \lambda^2 = 1 - \delta(\gamma - \delta), \quad (13)$$

737 and the phase lag equation, describing how the phase lag between HW and HWS
738 depends on wave celerity, convergence, and damping:

$$739 \quad \tan(\varepsilon) = \frac{\lambda}{\gamma - \delta}, \quad (14)$$

740 where q , b , and G account for the effect of river discharge and where:

$$741 \quad \beta = \theta - r_3 \zeta \varphi / (\mu \lambda), \quad \theta = 1 - (\sqrt{1 + \zeta} - 1) \varphi / (\mu \lambda), \quad \Gamma = \frac{1}{\pi} [p_1 - 2p_2 \varphi + p_3 \varphi^2 (3 + \mu^2 \lambda^2 / \varphi^2)].$$

742 (15)

743 Note that Γ is a friction factor obtained by using Chebyshev polynomials (Dronkers,
744 1964) to represent the non-linear friction term in the momentum equation:

$$745 \quad F = \frac{U |U|}{K^2 h^{-4/3}} \approx \frac{1}{K^2 h^{-4/3} \pi} (p_0 v^2 + p_1 v U + p_2 U^2 + p_3 U^3 / v) \quad (16)$$

746 in which U is the cross-sectional averaged velocity consisting of a steady component
747 U_r , generated by the fresh water discharge, and a time-dependent component U_t ,
748 introduced by the tide:

$$749 \quad U = U_r - U_t = v \sin(\omega t) - Q / \bar{A} \quad (17)$$

750 where Q is the fresh water discharge (treated as a constant during the tidal wave
751 propagation), and p_i ($i = 0, 1, 2, 3$) are the Chebyshev coefficients (see Dronkers, 1964,
752 p. 301), which are functions of the dimensionless river discharge φ through $\alpha = \arcsin(-$
753 $\varphi)$:



754
$$p_0 = -\frac{7}{120}\sin(2\alpha) + \frac{1}{24}\sin(6\alpha) - \frac{1}{60}\sin(8\alpha), \quad (18)$$

755
$$p_1 = \frac{7}{6}\sin(\alpha) - \frac{7}{30}(3\alpha) - \frac{7}{30}\sin(5\alpha) + \frac{1}{10}\sin(7\alpha), \quad (19)$$

756
$$p_2 = \pi - 2\alpha + \frac{1}{3}\sin(2\alpha) + \frac{19}{30}\sin(4\alpha) - \frac{1}{5}\sin(6\alpha), \quad (20)$$

757
$$p_3 = \frac{4}{3}\sin(\alpha) - \frac{2}{3}\sin(3\alpha) + \frac{2}{15}\sin(5\alpha). \quad (21)$$

758 The coefficients p_1 , p_2 , and p_3 determine the magnitudes of the linear, quadratic, and
759 cubic frictional interaction, respectively.

760